J Appl Physiol 102: 1244–1254, 2007;
doi:10.1152/japplphysiol.00738.2006.

HIGHLIGHTED TOPIC | *Physiological Imaging of the Lung*

Advances in magnetic resonance imaging of lung physiology

Susan R. Hopkins,[1,2] David L. Levin,[2] Kiarash Emami,[3] Stephen Kadlecek,[3] Jiangsheng Yu,[3] Masaru Ishii,[3] and Rahim R. Rizi[3]

Departments of [1]Medicine and [2]Radiology, University of California, San Diego, La Jolla, California; and [3]Department of Radiology, University of Pennsylvania School of Medicine, Philadelphia, Pennsylvania

Hopkins SR, Levin DL, Emami K, Kadlecek S, Yu J, Ishii M, Rizi RR. Advances in magnetic resonance imaging of lung physiology. *J Appl Physiol* 102: 1244–1254, 2007; doi:10.1152/japplphysiol.00738.2006.—This review presents an overview of some recent magnetic resonance imaging (MRI) techniques for measuring aspects of local physiology in the lung. MRI is noninvasive, relatively high resolution, and does not expose subjects to ionizing radiation. Conventional MRI of the lung suffers from low signal intensity caused by the low proton density and the large degree of microscopic field inhomogeneity that degrades the magnetic resonance signal and interferes with image acquisition. However, in recent years, there have been rapid advances in both hardware and software design, allowing these difficulties to be minimized. This review focuses on some newer techniques that measure regional perfusion, ventilation, gas diffusion, ventilation-to-perfusion ratio, partial pressure of oxygen, and lung water. These techniques include contrast-enhanced and arterial spin-labeling techniques for measuring perfusion, hyperpolarized gas techniques for measuring regional ventilation, and apparent diffusion coefficient and multiecho and gradient echo techniques for measuring proton density and lung water. Some of the major advantages and disadvantages of each technique are discussed. In addition, some of the physiological issues associated with making measurements are discussed, along with strategies for understanding large and complex data sets.

hyperpolarized helium-3 magnetic resonance imaging; regional ventilation; regional perfusion; apparent diffusion coefficient; ventilation-perfusion ratio; regional lung water

MANY PULMONARY DISORDERS ARE characterized by either an inability to supply fresh air to the exchange membrane (ventilation), an inability to supply blood to the membrane (perfusion), or an abnormality of the membrane itself, which hinders efficient gas diffusion. As one of the primary and most accessible activities of the lung, measurement of ventilation and lung volumes has been the focus of most pulmonary function tests, and spirometry is performed regularly to assess pulmonary integrity. Despite their usefulness, however, these global measures do not ultimately allow adequate characterization of disease heterogeneity; thus sensitivity to early and mild disease is lost, and the clinically relevant information for disease diagnosis and classification, as well as surgical planning, is incomplete. Developments in new imaging technologies in the past few decades have opened up new possibilities in acquiring regional information about the lung function and structure, with promise to address many of the intrinsic limitations of global measurements.

Shortly after the first axial X-ray computed tomograph became available in 1971, techniques were described that applied magnetic field gradients in three dimensions to create nuclear magnetic resonance (MR) images. The first images of two tubes of water were published in March 1973 (52). Since conventional MR imaging (MRI) exploits properties of protons in magnetic fields to produce images, the lung has historically presented problems, not only because it contains mostly air, and therefore signal is intrinsically low, but also because the many air-fluid interfaces contained in the lung degrade the MR signal, an effect known as susceptibility artifact. Nonetheless, great progress has been made in developing MR techniques in the lung that measure aspects of local physiology. In this review, some new techniques that are now available and suitable for pulmonary imaging are briefly discussed. Regional pulmonary perfusion, ventilation, gas diffusion, ventilation-to-perfusion ratio ($\dot{V}_A/\dot{Q}$), and lung water are some of the physiological measures that may be significantly altered by disease. By obtaining regional measures of these parameters, underlying mechanisms of disease can be explored, both in animal models and in intact humans. The ability to quantitatively evaluate such alterations in pulmonary function, particularly by measuring more than one variable, may provide insight into how pulmonary diseases affect lung function. The techniques described in this paper are extremely powerful and developing rapidly. With the use of perfusion, ventilation, gas exchange and lung water measurement techniques as illustrative exam-

Address for reprint requests and other correspondence: S. R. Hopkins, Associate Professor of Medicine and Radiology, Division of Physiology, Dept. of Medicine, Univ. of California San Diego, 9500 Gilman Dr., La Jolla, CA 92093 (e-mail: shopkins@ucsd.edu).

ples, the goal of this review is to briefly present a selection of the available MR techniques for performing these measurements, along with some of the issues associated with collecting, analyzing, and interpreting data.

PHYSIOLOGICAL ISSUES FOR LUNG IMAGING

Partitioning of Ventilation, Blood Flow, and Water in the Lung

The primary function of the lung is to act as a gas exchanger, and the matching of ventilation and perfusion is important to optimize efficiency of gas exchange. Perfusion is a general term describing the delivery of arterial blood to a capillary bed, whereas blood flow is the rate of delivery of arterial blood to the capillary bed in a known mass of tissue (13). Ventilation can be similarly defined as the exchange of gas in the lung, whereas alveolar ventilation is a measure of the amount of fresh gas supplied to the alveoli. Some of the techniques described in this paper provide an image of the distribution of ventilation and perfusion and contain information from airways and blood vessels in a variety of sizes, not just capillaries and alveoli, and therefore do not strictly represent alveolar ventilation or perfusion. From an anatomical standpoint, most of the pulmonary blood volume is contained in relatively large vessels, arteries, arterioles, venules, and veins, and, even when maximally recruited during exercise, pulmonary capillary blood volume is <20% of the total pulmonary blood volume (45). Conversely, most of the lung air volume is contained within the alveoli, so anatomical dead space is small compared with the regions of the lung that do participate in gas exchange. Since the resolution of the techniques described in this review is less than required to image individual alveoli and capillaries, the information obtained must be carefully evaluated. This is particularly important when describing heterogeneity, since the heterogeneity of a system is dependent on the scale of measurement, as well as the resolution level (30). The lung by weight is ~80% water, roughly split between intravascular and extravascular spaces. Since the partitioning of total lung water between these two spaces can be altered by a number of physiological and pathological processes, it is important to account for any changes when drawing conclusions from measures of total lung water.

Respiratory and Cardiac Cycles

Unlike studies in other organs, the need for the subjects to breathe requires respiratory gating or limits lung acquisition times to a breath hold. If total lung capacity is employed for the breath hold, while this increases the time a subject is able to breath hold (89), allowing longer acquisition times, it decreases the measured signal in studies imaging blood flow or lung water, since each voxel will contain more air and less protons from lung tissue. Blood flow in the lung is pulsatile; therefore, for some types of perfusion scanning, it is necessary to cardiac gate the scanning and trigger to the ECG signal (9). While technically this does not present a problem with healthy normal subjects, subject with cardiac arrhythmias, such as atrial fibrillation, can present considerable difficulty. Blood gases are altered by breath holding (78). These changes are of sufficient magnitude to be physiologically important if the duration of exposure is long enough and may thus alter hypoxic pulmonary vasoconstriction (83) and therefore regional distribution of perfusion. The P_{O_2} alterations induced by breath holding are unlikely to have a significant effect on regional perfusion, since hypoxic pulmonary vasoconstriction requires at least 20 min to become maximal (78), and breath hold times are much shorter. However, the pulmonary vascular response to CO_2 is less well studied and may perhaps be more important during breath holding, as the half-time for the maximal pulmonary vascular response is ~90 s (83). Thus small changes in perfusion resulting from the increased concentrations of CO_2 during breath-hold scanning are possible. Regional pulmonary perfusion and $\dot{V}_A/\dot{Q}$ are also affected by lung volume, and perfusion is more uniform in humans at low lung volumes (5). In addition to the possibility of altering lung function by the measurement, this has the potential to limit the ability to compare between successive images, unless lung volumes are standardized, or unless some internal standard is available.

Posture

MR scanners designed for clinical imaging of patients have a horizontal bore and permit only prone, semiprone, and supine postures. Functional differences between prone and supine postures need to be considered; for example, blood flow and $\dot{V}_A/\dot{Q}$ heterogeneity are more uniform in the prone posture (68). Gravity has an influence on the distribution of pulmonary perfusion, lung density, and alveolar size (11, 12, 29) that is dependent on posture (51), and the prone and supine postures differ both from one another and also from the upright posture (51). The extent of this gravitationally based influence is the subject of considerable debate (31, 32, 87). The effects of gravity on pulmonary perfusion vary with lung volume, with the largest effect at total lung capacity and the smallest effect at residual volume (43). Regional ventilation has also been shown to exhibit strong dependence on subject's posture (60): in the supine posture, ventilation varies with a gradient from dorsal to ventral regions, whereas, in the prone posture, this distribution is significantly more uniform. All of these factors must be considered when comparing results between studies that may offer conflicting information.

THE CHALLENGE OF VALIDATION

As new techniques are developed and applied to answer biologically meaningful questions, important issues relate to reliability of the techniques. Reliability, the ability of a measurement to give the same value when repeated under the same conditions, is easily established by making a number of repeated measurements in the subject population of interest. However, establishing validity, and resolving the question of how well does a technique measure what it purports to measure, is much more challenging. Many of these innovative techniques lack a standard to which they can be fully compared. This is not a new problem. For example, the multiple inert-gas elimination technique, based on simple principles of mass balance, while widely held as the gold standard for determining $\dot{V}_A/\dot{Q}$ heterogeneity, was never directly validated. However, by providing numbers that made physiological sense and withstanding intense scrutiny over time, it has gradually become accepted.

In validating these new techniques, multiple approaches are needed. The first is to determine whether the data agree with

what is expected from established measurements. Measures of regional pulmonary perfusion may be considered as an example: the volume (gas and tissue) of a normal human lung at functional residual capacity is ~3,000–4,000 ml on average, and cardiac output at rest is ~5,000–6,000 ml/min. Therefore, regional perfusion of the lung should be ~1.3–2.0 $ml \cdot min^{-1} \cdot ml^{-1}$ in a resting, normal subject. A second step might be to measure, preferably simultaneously, cardiac output and perfusion in the entire lung in a group of subjects and determine agreement. However, this will not give measurements of heterogeneity or regional information, which is one of the real advantages of these new measurements. The third step might be to cross-validate the technique against other techniques offering spatial information. This last step is challenging, because the ideal comparison technique should measure the same thing as the technique to be validated and should not be subject to significant measurement error itself. For example, measurements of perfusion in the lung made with microspheres, although well established as highly accurate, will not reflect any effect that regional variations in lung density in situ will have on the measurement of regional perfusion using external imaging techniques such as MRI, which measure perfusion per voxel (i.e., per unit volume) rather than per gram of tissue.

SPECIFIC MRI TECHNIQUES

Regional Perfusion

The measurement of pulmonary blood flow using MRI techniques is difficult. In addition to the previously discussed issues of low proton density and local magnetic field inhomogeneity, cardiac motion and the pulsatility of pulmonary blood flow can significantly affect measurements. All of these issues need to be considered when designing methods to study pulmonary blood flow. In general, two types of MR sequences can be used to evaluate pulmonary blood flow, each with its advantages and disadvantages. The first method is known as bolus tracking or dynamic contrast-enhanced imaging, where multiple images are acquired rapidly as intravascular contrast travels through the pulmonary circulation (54). The second technique, using methods collectively known as arterial spin labeling (ASL) (13), does not require intravenous contrast material, but instead, magnetically "tags" inflowing blood.

Dynamic contrast-enhanced MRI. With this technique, multiple images are acquired rapidly, either of a single plane through the lung parenchyma (two-dimensional) or of the entire lung (three-dimensional) during a bolus of an intravenous contrast agent, such as gadopentetate dimeglumine. With the use of an appropriate MR sequence, an increase in the signal intensity of the lung parenchyma is seen as contrast passes through the pulmonary vasculature (Fig. 1). Regions of decreased parenchymal blood flow will be identified qualitatively as areas of poor regional contrast enhancement. Quantitative estimates of pulmonary perfusion can then be obtained by applying indicator dilution techniques to the change in signal intensity seen over time for a given region of the lung (Fig. 2). Following a brief transit delay, a sharp rise in signal intensity is seen with the arrival of contrast, and the signal intensity will decline as the contrast washes out from the region of interest (ROI). The first-pass portion of the curve can be fit to a gamma-variate function (84). From this, quantitative values for blood volume, blood flow, and mean transit time (MTT) can be obtained (84, 90).

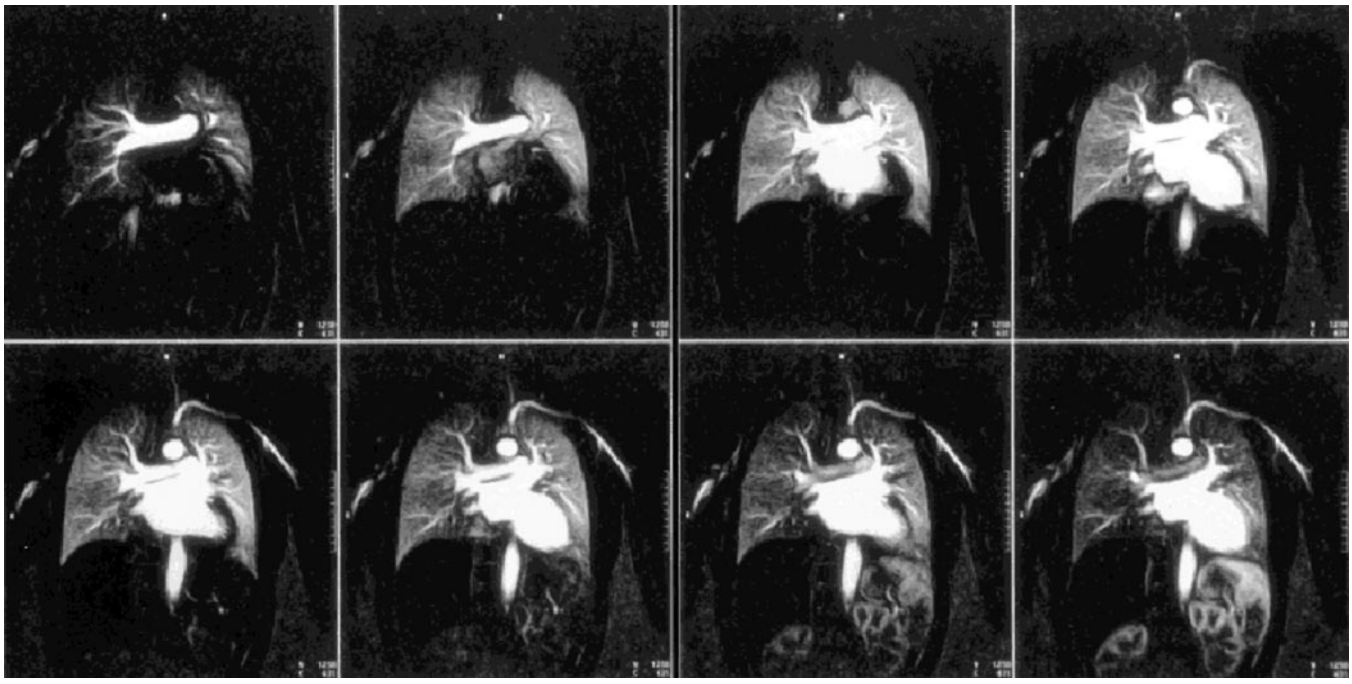

Fig. 1. Raw images of dynamic contrast-enhanced magnetic resonance (MR) imaging of pulmonary perfusion in a normal volunteer. Eight consecutive coronal images are shown from the total of 45 coronal images obtained every 1 s in the plane of the pulmonary hila. The pulmonary arterial tree was visualized beyond the segmental branches, followed by diffuse blush of lung parenchyma. A gradual increase in signal intensity of the lung parenchyma is observed, and, as contrast reaches the systemic circulation, the descending aorta and renal and splenic perfusion is observed. [Borrowed with permission (37).]

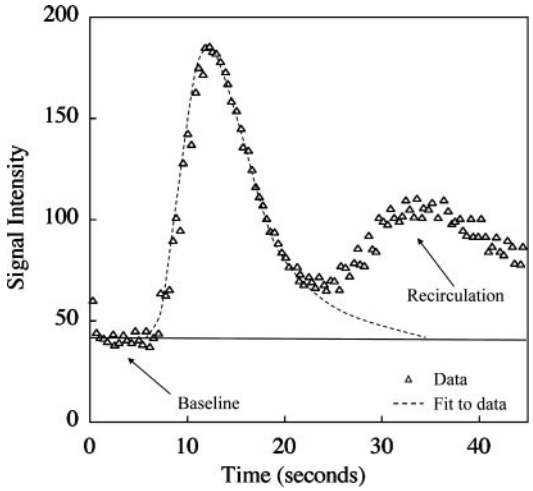

Fig. 2. Signal intensity in a normal volunteer within a region of interest in lung parenchyma following bolus injection of contrast during dynamic contrast-enhanced MR imaging of pulmonary perfusion. After a transit delay, a sharp rise in signal intensity is followed by rapid washout. The late peak reflects recirculation of indicator into the region of interest. After gamma-variate fitting, the first moment of the curve represents mean transit time, and area under the curve represents blood volume of the region of interest. [Adapted from Ref. 55.]

There are several advantages of dynamic contrast-enhanced MRI. It is relatively straightforward to implement and has a spatial resolution that is typically better than that of ASL. It also can provide a direct measurement of blood volume and can demonstrate the patterns of perfusion over time within the lungs. There are several disadvantages, however. The use of intravenous contrast limits the number of repeated measures, as the contrast bolus has to be cleared from the blood before reimaging. This eliminates the ability to make duplicate measures at a single time point and significantly reduces the ability to evaluate changes in physiology that might occur over a short time period. The number of measurements that can be made is also limited by the total amount of contrast material that can be given over a 24-h period (10, 23, 79). While regional blood volume is accurately determined directly from the area under the observed tissue concentration curve, the indicator dilution technique calculation of regional blood flow and MTT is less straightforward and may be subject to substantial error. The central volume principle relates blood volume, blood flow, and MTT through a vascular bed. In this approach, the MTT is the first moment of the contrast curve for a draining vessel. However, this is not strictly true for data obtained from the vascular bed itself, such as is obtained with MRI (86), and thus both MTT and blood flow are prone to error. Researchers have, however, demonstrated a good correlation between regional blood flow measured using this technique and blood flow measured using colored microspheres, suggesting that this limitation may be relatively small (37).

ASL. ASL MRI techniques have been used to quantify regional perfusion in many organ systems (27, 73, 91). The two primary advantages of ASL sequences are that regional blood flow can be determined directly from the signal intensity of the perfusion image, and no intravenous contrast is needed.

A specific type of ASL technique (9, 58) that allows for quantification of regional pulmonary perfusion during a single breath hold is ASL-FAIRER [FAIRER stands for flow-sensitive alternating inversion recovery with an extra radio frequency (RF) pulse]. Essentially, ASL techniques use RF pulses to invert the magnetization of protons traveling within the blood, allowing them to act as an endogenous tracer for the evaluation of blood flow. During each breath hold, two images are obtained: a selectively and nonselectively tagged image. The selectively tagged image is acquired by applying a selective inversion pulse only to the slice of interest. This pulse inverts the magnetization of all spins within the slice (blood plus extravascular tissue), and, following a delay that includes one cardiac cycle, the "selective" image is acquired. During this delay, fully relaxed spins move into the slice, replacing inverted spins that flow out of the slice. The nonselective tagged image is acquired by applying a nonselective inversion pulse to the entire chest, so that the magnetization of arterial blood outside the slice, as well as the blood and extravascular spins within the slice, are inverted. After waiting for the same period of time, the "nonselective" image is acquired. If this is done carefully, then in each image the spins that were in the slice at the beginning of the experiment, and remained there until the image was acquired, will generate identical signals, whereas the magnetization of the arterial blood that entered the slice during the delay will be fully relaxed in the selective image and inverted in the nonselective image. Subtraction of the two images then yields an image of just the arterial blood delivered to the imaged slice during the delay interval (Fig. 3). In practice, all inverted magnetizations partially relax back toward equilibrium during the delay interval, and this sets a practical limit on how long that delay can be. That is, the "tagged" magnetization has a finite lifetime set by the longitudinal relaxation time of blood. Since this technique involves movement of blood from regions of lung immediately adjacent

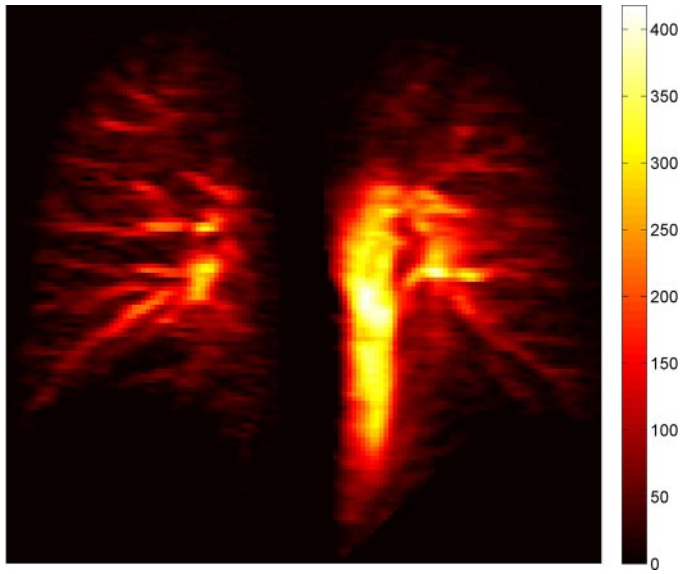

Fig. 3. A single-slice coronal image of pulmonary perfusion in a healthy, normal volunteer imaged using arterial spin labeling-flow-sensitive alternating inversion recovery with an extra radio frequency pulse (ASL-FAIRER) to magnetically tag protons for use as an endogenous tracer. Signal intensity is a function of protons delivered (flow) during the interval between tag and image acquisition, and with appropriate doped water phantoms absolute quantification of regional perfusion is possible. The data from this study were collected as part of a study approved by the University of California, San Diego Human Subjects Research Protection Program.

to the imaging slice, the effective transit times for tagged blood is short, and errors caused by signal decay are minimized (9). Absolute or relative quantification of blood flow can be obtained from this image (Fig. 4). One of the limitations of the ASL technique is that it only provides information on perfusion: it does not measure blood volume or transit time. It has the advantage that measurements can be made repeatedly over very short time periods (seconds). The absence of contrast also means that the measurements can be repeated indefinitely. It is somewhat more difficult to implement compared with dynamic contrast-enhanced imaging.

ASL measurements of regional pulmonary perfusion have been used to demonstrate increases in pulmonary flow heterogeneity in subjects who have previously suffered high-altitude pulmonary edema (HAPE), a potential fatal disease associated with rapid travel to high altitude (41). It has been hypothesized that hypoxic pulmonary vasoconstriction may be nonuniform in HAPE, an idea supported by the work of Hlastala et al. in mammalian lungs (40). The ASL data suggest this process may be fundamentally different in HAPE-susceptible individuals, at least after they have developed HAPE on one occasion, providing insight into the inciting mechanism of the disease. Similar changes in perfusion heterogeneity are found using 1 h of steep head-down tilt (39), which alters ventilatory inhomogeneity (22) and suggests that regional pulmonary function is altered in subclinical edema, even in the absence of overt disease.

Hyperpolarized Gas MRI

Hyperpolarized gases. Hyperpolarization refers to a process in which magnetically active nuclei are aligned to a degree many orders of magnitude greater than is normally achievable under in vivo conditions. These nuclei, typically in the gas state, are then administered into the lungs and imaged before they have a chance to return to the thermal equilibrium conditions dictated by body temperature and the local magnetic field. As an example, the polarization level of ^{3}He can be increased to as high as 10^{5} times the thermal polarization of water molecules, the source of conventional MRI signal. This increased signal, along with the complete lack of indigenous background, compensates for the low concentration of gas molecules in airways and, therefore, can be used for higher spatial or temporal resolution imaging. The first hyperpolarized gas MR image was acquired by Albert et al. (2) using ^{129}Xe in a mouse lung, and later by MacFall et al. (56) in human lungs using ^{3}He. These two gases have become common choices for medical imaging, primarily because of their biological inertness (with the exception of anesthetic effects of ^{129}Xe) and their great potential to elucidate lung function and structure.

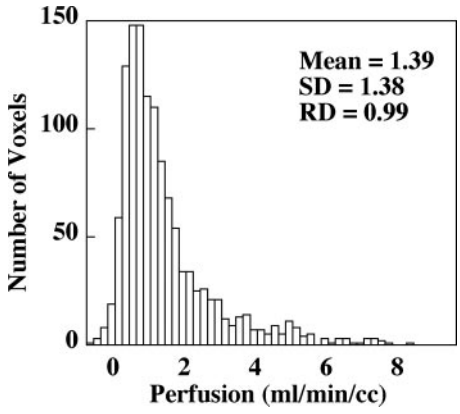

Fig. 4. Histogram of mean perfusion from the right lung of the image presented in Fig. 3, after absolute quantification. The relative dispersion (RD) is 0.99, similar to that reported for normal subjects (39, 41).

Hyperpolarization methods. One of the most widely used methods to impart nuclear alignment to gas is by spin exchange optical pumping (35, 36, 53, 85) of an alkali metal vapor, whereby the mixture of the noble gas and these metal particles is illuminated with resonant, polarized light, as originally proposed by Kastler (46). This method is applicable to both ^{3}He and ^{129}Xe nuclei. Metastability exchange optical pumping method, originally proposed by Colegrove et al. (15), on the other hand, is a more efficient method for polarizing ^{3}He, especially for large quantities of polarized gas, but its application is limited to this specific nucleus (1, 28). The magnetic properties and extreme chemical inertness of ^{3}He leads to higher polarization, longer storage time, improved visualization of surrounding structure, and a very attractive safety profile. ^{129}Xe, on the other hand, polarizes faster and is soluble in blood with several other possible properties and applications, as discussed in the references (21, 50, 59, 65, 74).

Hardware requirements. In addition to nucleus-specific chest RF coils, imaging hyperpolarized nuclei requires broadband MR scanners capable of performing acquisition at frequencies different from the conventional proton (^{1}H) MRI commonly available in medical institutions. As potential clinical applications of multinucleus MRI techniques are expanding, many manufacturers have started providing broadband capabilities to both existing scanners and new models. Moreover, the relatively fast in vivo depolarization rates of hyperpolarized nuclei [in the order of 10~20 s (66)] and the lack of magnetization recovery demands that images be acquired with a fast pulse sequence, such as gradient echo or echo planar sequences.

Regional Ventilation

Several different techniques for regional measurement of ventilation have been proposed, and some have found clinical application. The most common approach makes use of an inhaled radionuclide (typically ^{133}Xe, ^{81}Kr, or aerosolized Tc), and the gas distribution inside the lung is imaged with a gamma camera. Other proposed schemes use inhaled ^{13}N and PET, or a radiodense gas (typically stable Xe) and standard X-ray, computed tomograph, or synchrotron radiation (7). MR-based techniques include MRI of aerosolized contrast agents such as gadolinium-diethylenetriamine pentaacetic acid (8, 33, 47, 64, 81, 82) and oxygen-enhanced MRI as a measure of ventilation (6, 20, 44, 57, 69–71, 93).

Each of the above techniques has advantages and limitations of its own. Notable limits include achievable resolution (either inherent or because of limited signal-to-noise), exposure to ionizing radiation, and/or problems with cost or availability in a clinical setting. The gadolinium-diethylenetriamine pentaacetic acid particle size and the long administration time (in the order of a few minutes) could be prohibitive in certain types of airway diseases. Oxygen-enhanced MRI reflects a combination of ventilation, membrane function, and perfusion effects in the

lung. For this reason, considerable effort over the last decade has gone into the development of signal-enhancing techniques capable of measuring regional ventilation minimally affected by other pulmonary processes in the lung. The promising sensitivity and safety characteristics of hyperpolarized gas MRI have, therefore, proved to be a suitable tool for further development in this field and have been used for qualitative ventilation studies (48, 49), ventilation defects in asthmatic patients (4, 77), and to generate high-resolution ventilation maps (65).

In direct analogy with the radionuclide methods, the measured signal in each imaging voxel is proportional to the polarization level and concentration of the gas. Fractional ventilation r is then defined as the amount of gas added to a ROI during inspiration ($\dot{V}_{new}$) normalized by the total gas space of that ROI at the end of inspiration ($\dot{V}_{total}$):

$$r = \frac{\dot{V}_{new}}{\dot{V}_{total}} = \frac{\dot{V}_{new}}{\dot{V}_{new} + \dot{V}_{old}} \quad (1)$$

The total volume of the ROI at end inspiration, therefore, consists of a fraction r of fresh gas plus a fraction $q = 1 - r$ of residual gas. Fractional ventilation can, therefore, be altered by any pulmonary disease affecting the natural flow of air entering (e.g., asthma) or leaving (e.g., emphysema) airways. A technique to measure fractional ventilation was originally proposed by Deninger et al. in guinea pigs (19). This technique consists of acquiring images after administering a consecutively increasing number of hyperpolarized ^{3}He gas breaths (34). For a given sequence of hyperpolarized helium breaths, signal (or equivalently the concentration of the new incoming gas) in a high-r (well-ventilated) region rises at a faster rate than that of a low-r (poorly ventilated) region, and, therefore, fewer breaths are required to completely exchange the gas in this region. Performing the signal buildup analysis on a voxel-by-voxel basis yields the regional ventilation map for the entire lung. Figure 5 shows a typical map of regional fractional ventilation in a coronal slice of a healthy rat lung, along with the respective frequency distribution histogram. The high-gas transport efficiency of conductive airways is depicted in their high-fractional ventilation ($r > 0.7$). The average r in this slice, excluding the trachea, was measured as 0.29 ± 0.04.

HELIUM DIFFUSION AS A MEASURE OF LUNG MICROSTRUCTURE

The ^{3}He atoms in a gas perform a Brownian random motion. The average traveled distance of the gas atoms during a given duration of time is determined by the diffusion coefficient D, specific to the gas or gas mixture. For pure ^{3}He gas under standard conditions (and without restricting wall and barriers), D is 2.05 cm^2/s (14) and ~0.88 cm^2/s in an atmospheric concentration (92). If gas diffusion in the lung is measured, however, we find that D is much smaller than predicted from free diffusion and is not homogeneous. The bulk of this difference and the heterogeneity indicate diffusion hindrance by the lung structure itself; thus the measured value of D is termed the apparent diffusion coefficient (ADC). ADC measurements are, therefore, a measure that is altered by changes in the lung microstructure and give information about changes in function. ADC appears to be a sensitive (76) and reproducible (67) marker for early detection (25, 76) and progression (75) of disease and other processes affecting the size of alveoli and small airways (92).

The simplest MR technique for measuring ADC, originally proposed by Stejskal (80), is based on applying a symmetric bipolar gradient before acquiring the image. The pair of gradients separated with an intermediate time delay dephase and rephase the nuclei. In the presence of diffusion, or motion of atoms, the rephasing will be incomplete, resulting in a signal loss proportional to the D. Figure 6 shows a set of ADC measurements in three slices of the lung of a healthy human subject in the supine position. The mean ADC value is centered around 0.16 cm^2/s with a posterior-anterior gradient.

Hyperpolarized ^{3}He MRI has compared ventilation defects in patients with cystic fibrosis before and after treatment to healthy subjects. Even the cystic fibrosis patients with normal spirometry had significantly more ventilation defects than healthy subjects, and these defects were correlated with changes after treatment (63). Hyperpolarized ^{3}He MR has also been used to evaluate the ADC and thus estimate peripheral air space size in normal subjects of different ages and patients with emphysema. The ADC is increased with increasing age (24), is larger in active and passive smokers than in healthy never-smokers (25), and is larger in patients with emphysema (25, 76). Thus this technique may provide insights into early diagnosis of airway disease or response to treatment.

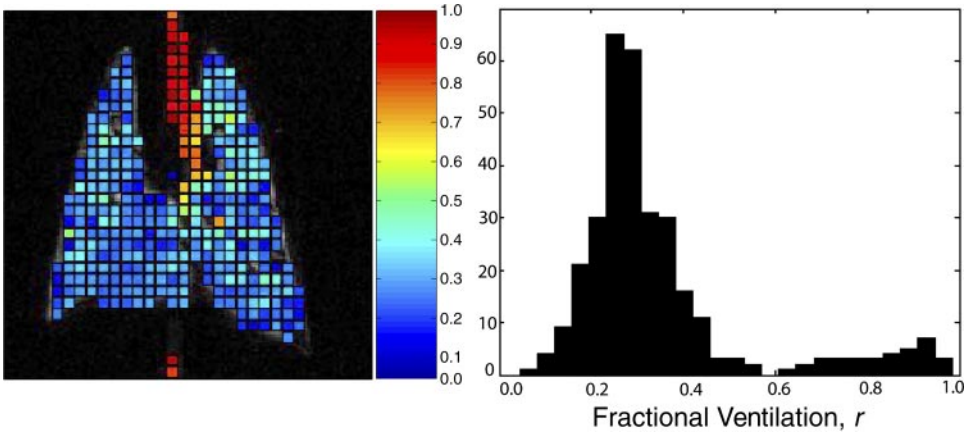

Fig. 5. Regional measurement of fractional ventilation in a coronal slice of a healthy rat lung. As can be seen, conductive airways show a relatively high $r > 0.7$, representing very efficient gas transport in these regions. The value of r in the lung parenchyma is homogeneously distributed in the range of 0.2~0.4. Images were acquired using a fast multislice gradient echo pulse sequence with repetition time/echo time = 6.6/3.3 ms, field of view = 5×5 cm^2, slice thickness = 4 mm, flip angle $\alpha = 10°$, and matrix size of 128×128 pixels. All animal studies were performed in accordance with a protocol approved by the Institutional Animal Care and Use Committee of University of Pennsylvania.

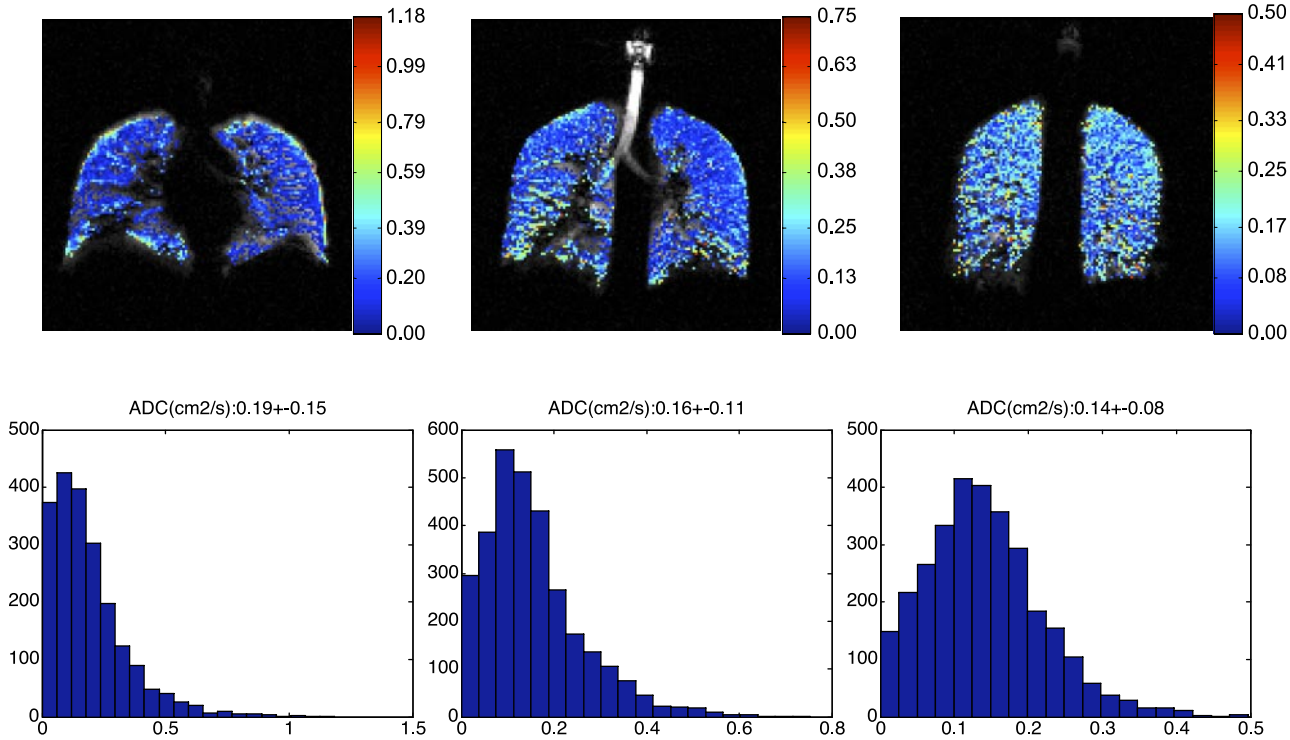

Fig. 6. Apparent diffusion coefficient (ADC) maps in three slices of a healthy human lung. The ADC is distributed around 0.16 with a posterior-anterior gradient. Imaging parameters: echo time/repetition time = 6.5/10 ms, field of view = 35 × 35 cm, slice thickness = 30 mm, α = 3~4°, matrix size = 128 × 128 pixels, and *b* values = 1.73, 1.15, 0.71, 0.33, and 0.0 s/cm^2. All human studies were performed in accordance with a protocol approved by the Institutional Review Board of University of Pennsylvania.

Regional Partial Pressure of Oxygen and $\dot{V}_A/\dot{Q}$

Hyperpolarized ^{3}He spins lose polarization in the presence of oxygen due to dipolar coupling between the nuclear and molecular magnetic moments during collisions. This relaxation happens at a rate proportional to the absolute oxygen concentration, so the effect can serve as a marker for measurement of certain aspects of lung function. Since the rate at which oxygen is taken up into the bloodstream is approximately constant during typical durations of alveolar oxygen pressure ($P_{A_{O_2}}$) measurements (88), $P_{A_{O_2}}$ can be assumed to change linearly with time. Therefore, in the absence of any other significant relaxation mechanisms, the ^{3}He MRI signal can be expressed as a first-order process:

$$S(t) = S(0) - \Gamma \cdot P_A O_2 \cdot t + \frac{1}{2} R \cdot t^2 \qquad (2)$$

where S is the MRI signal intensity, R is the rate of oxygen uptake into the blood (the O_2-depletion rate), and Γ is the constant of proportionality between oxygen pressure and ^{3}He relaxation rate.

Based on the original work of Eberle et al. (22), several schemes for in vivo measurement of regional partial pressure of oxygen in the lung have been proposed. These techniques are based on acquiring a series of images during either one (17, 26) or two (18) breath holds. Measurements requiring two breath holds suffer from coregistration problems and longer acquisition times, making single-acquisition sequences a more desirable technique for daily clinical scans. These methods can be naturally extended to multislice acquisitions. Figure 7*A* shows representative $P_{A_{O_2}}$ measurements in three slices of a healthy pig lung. A mixture of hyperpolarized ^{3}He and O_2 with a ratio of 4:1 was used, and measurements were performed using a single-acquisition sequence. The average $P_{A_{O_2}}$ in *slices 1–3* was measured as 101 ± 22, 93 ± 12, and 87 ± 11 Torr, respectively. The results averaged over all three slices resulted in a $P_{A_{O_2}}$ value of 92 ± 15 Torr.

Determination of Regional $\dot{V}_A/\dot{Q}$ from $P_{A_{O_2}}$ Measurements

A technique recently developed by Rizi et al. (72) permits the calculation of regional $\dot{V}_A/\dot{Q}$ from measured $P_{A_{O_2}}$ on a regional basis. This technique is based on what is termed the forward problem, which uses measured $\dot{V}_A/\dot{Q}$ distributions to predict overall pulmonary gas exchange. The forward problem uses known values for $\dot{V}_A/\dot{Q}$, inspired oxygen fraction, mixed-venous P_{O_2}, and mixed-venous P_{CO_2} to calculate unknown alveolar gas tensions [$P_{A_{O_2}}$ and alveolar CO_2 tension ($P_{A_{CO_2}}$)]. In this technique, however, the forward problem is modified to calculate $\dot{V}_A/\dot{Q}$ from local $P_{A_{O_2}}$ measurements. This so-called inverse problem employs well-established equations of steady-state exchange of O_2, CO_2, and N_2 to determine the local $\dot{V}_A/\dot{Q}$. Like the forward problem, the inverse problem begins with the steady-state mass balances for gas exchange, which results in four equations in four unknowns: $P_{A_{O_2}}$, $P_{A_{CO_2}}$, the ratio of inspired ventilation to local perfusion, and alveolar N_2 tension. In the forward problem, these equations are reduced to two equations in two unknowns ($\dot{V}_A/\dot{Q}$ and $P_{A_{CO_2}}$), while in the inverse problem, the four equations are reduced to one equation in one unknown ($P_{A_{CO_2}}$). The resulting $P_{A_{CO_2}}$ is then

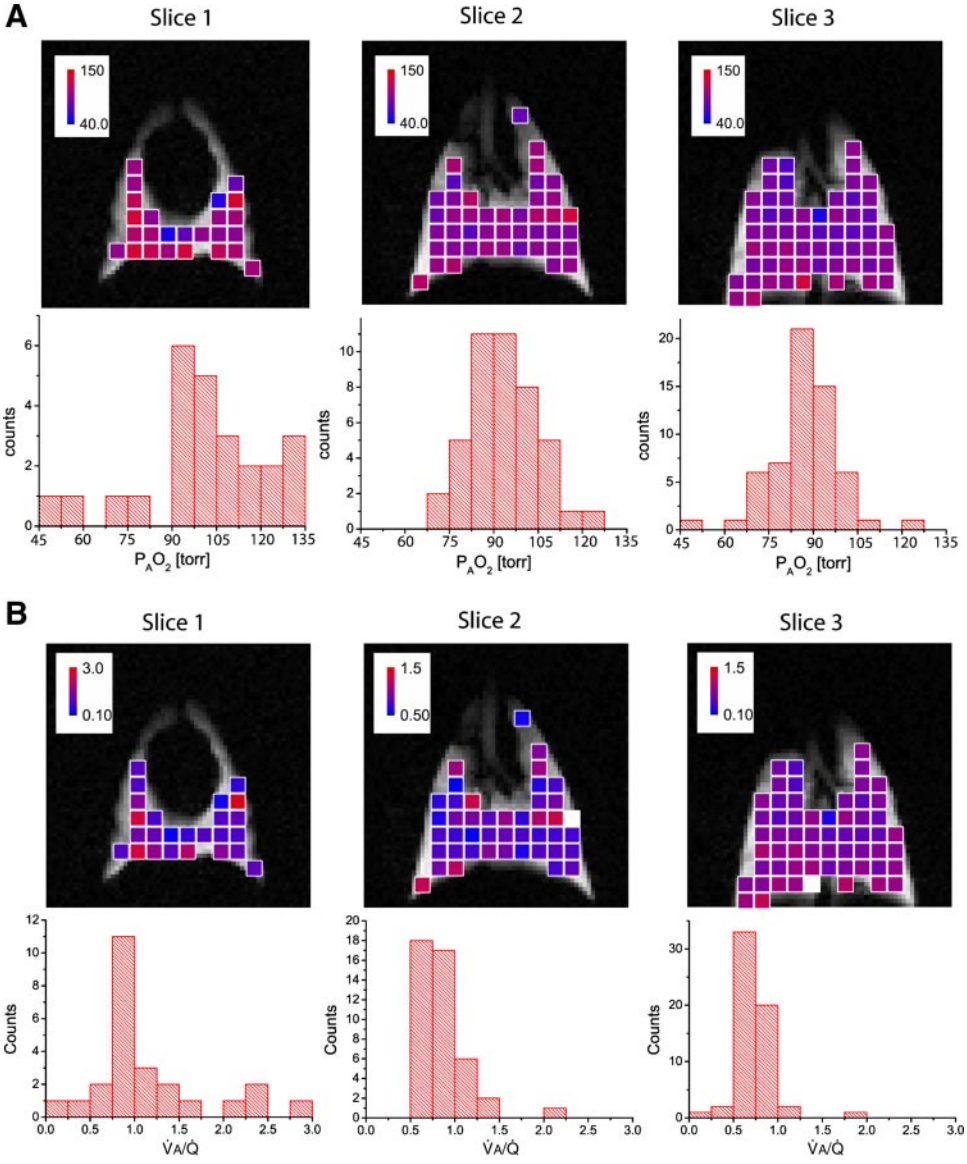

Fig. 7. *A*: distribution of alveolar O_2 tension ($P_{A_{O_2}}$) in the normal pig lung for three slices. The single-acquisition sequence was performed with an acquisition time $\Delta\tau = 0.4$ s and an interscan time delay $\tau = 6$ s. Six images for each of the three slices were analyzed by binning 4×4 voxels. White squares indicate values <70 Torr. Bin size in the histograms is 7.5 Torr. *B*: distribution of ventilation-to-perfusion ratio ($\dot{V}_A/\dot{Q}$) in the normal pig lung for three slices, corresponding to those shown in *A*. White squares indicate values <0.5. Black squares indicated values >1.5. Bin size in the histograms is 0.25. All animal studies were performed in accordance with a protocol approved by the Institutional Animal Care and Use Committee of University of Pennsylvania.

inserted into one of the equations used in the forward problem to calculate $\dot{V}_A/\dot{Q}$ (72).

The regional $\dot{V}_A/\dot{Q}$ was calculated for the same pig for which $P_{A_{O_2}}$ maps are presented in Fig. 7*A*. With the use of published $P_{A_{O_2}}$ to $\dot{V}_A/\dot{Q}$ mappings, $\dot{V}_A/\dot{Q}$ maps for each oxygen data point were calculated, as shown in Fig. 7*B*. The average $\dot{V}_A/\dot{Q}$ in *slices 1–3* was measured to be 1.15 ± 0.65, 0.85 ± 0.27, and 0.74 ± 0.21, respectively. The results averaged over all three slices resulted in a $\dot{V}_A/\dot{Q}$ value of 0.86 ± 0.38.

Regional Lung Water

Changes in pulmonary fluid balance have the potential to significantly affect gas exchange by thickening the gas exchange barrier and by altering local blood flow. Regional lung water can be altered by a number of conditions, including hypoxia, exercise, and cardiopulmonary disease. The measurement of lung water was one of the earliest applications of MR, preceding many of the clinical imaging applications (16, 38). The principles behind the estimation of lung water are based on the fact that the signal intensity of any MR image is related, in part, to the number of protons present. With the use of an appropriate imaging scheme, however, the image signal intensity can relate almost exclusively to proton density. The most common approach is the use of a multiecho sequence. MR signal decreases exponentially with time, and if image signal intensity following a single RF pulse is determined at multiple time points (multiple "echoes") over a very rapid time frame (milliseconds), the exponential decay curve can be determined. The signal intensity extrapolated back to a time of zero will be related only to proton density. If a similarly derived signal intensity is also known for a sample of water, then the ratio of signal intensities will give the amount of water present for any ROI. This method has compared with lung water determined gravimetrically by several investigators. Cutillo et al. (16) found the two measures to be highly correlated with an absolute difference of typically <20%. However, more recently, Mayo et al. (61) found that MR typically underestimated the amount of lung water by 5% compared with gravimetric

techniques. The differences between these two studies may relate to significant improvements in MR hardware and sequence design in the decade between the two studies.

Alternately, the amount of water present in a ROI can be estimated from a single time point using a sequence where the measured signal intensity is dominated by proton density. An example is a gradient echo sequence with a very short echo time and very small flip angle, which acts to maximize the correlation between proton density and signal intensity. This approach has several advantages. It is an easier sequence to design and implement, and data acquisition is slightly faster, allowing for shorter breath-hold times. Again, a comparison is made to the signal intensity of a sample of water, and the ratio of signal intensities is used to determine water content. To the extent that other factors, such as local magnetic field inhomogeneity within the lung parenchyma, affect the measured signal intensity, error will be introduced in the determination of regional lung water.

Measurements of regional lung water have been made in endurance-trained athletes, who develop gas exchange limitations during and following exercise. In these individuals, it has been suggested that the increase in $\dot{V}_A/\dot{Q}$ inequality observed is due to interstitial pulmonary edema (42). With the use of a multiecho sequence to measure regional lung water following intense, sustained exercise, an increase in lung water was observed. This was most likely due to interstitial fluid accumulation (62), since, by waiting for 1 h after exercise for the acute blood volume shifts to resolve before making measurements, by masking out large vessels and measuring the changes in pulmonary capillary blood volume, the intravascular shifts were accounted for or excluded.

APPROACHES TO DATA ANALYSIS

MR data sets are extremely large and generate roughly 100,000 voxels per lung. A significant issue is how to evaluate and express this large data set to compare among subjects and across interventions. A detailed discussion of data analysis techniques is beyond the scope of this review, and the reader is referred to a review by Glenny (30) for more information on analysis of lung spatial data. Some of the data evaluation techniques briefly described below provide numbers that describe the heterogeneity of a system and are therefore useful for statistical analyses and also provide anatomic information as to the scale of heterogeneity, the size of related areas, and, in some cases (cluster analysis), the anatomic location. However, it is clear that developing techniques to evaluate spatial information in the lung will occupy researchers for some years to come.

The relative dispersion (standard deviation/mean, also known as the coefficient of variation) can be used to characterize spatial heterogeneity of information, with higher values representing more heterogeneously distributed systems (Fig. 4). The relative dispersion is a useful measure for globally quantifying the extent of spatial heterogeneity, but the obvious disadvantage is that the measure eliminates any anatomic information. Nevertheless, being able to quantitatively characterize one data set as having a different heterogeneity than another has been shown to be a useful tool (39, 41). Spatial correlation provides another means of quantitatively comparing the nature of the spatial information contained in an image. In this method, the correlation coefficient is determined for the data of interest for all locations within the lung that are separated by a given distance. The correlation coefficient can then be recalculated for all pairs of points separated by a greater distance, and this is repeated to generate a curve of correlation coefficient r vs. separation distance. The zero-crossing point (distance of zero correlation) is a measure of the scale of the major components of the heterogeneity within the image (30).

Other approaches that have been used to evaluate spatial information in the lung include fractal analysis and cluster analysis (30). Within the lung, blood flow in one region is correlated with flow in adjacent regions of the lung. To be fractal in nature, this relationship must hold for all regions, regardless of size or location. The fractal dimension statistic is calculated by taking the relative dispersion of the image after smoothing with progressively larger blocks (e.g., 1, 9, 25. . . voxels averaged) centered on each voxel (3). The slope of the curve is calculated, and the fractal dimension is calculated. Cluster analysis is a statistical method for grouping items, such as pieces of lung, into "clusters" that share similar characteristics, such as response to a given stimulus. The entire clustering process is completed without reference to the spatial location of any lung region, and then, once identified by their response, the anatomic location of these pieces is determined. The mean Euclidean distance between all possible pairs of cluster members can be used to describe the size of the clusters, becoming smaller as the clusters become spatially more compact.

CONCLUSIONS

In the preceding pages, a variety of recent MRI techniques have been presented that allow assessment of regional lung function. A full understanding of these powerful techniques will require multidisciplinary teams with skills in radiology, MR physics, and physiology. As these techniques become more widely available, they offer great potential to answer meaningful questions in medicine and biology, not only about lung structure but also lung function, allowing mechanistic insights.

ACKNOWLEDGMENTS

The helpful insights of A. Cortney Henderson, G. Kim Prisk, and Richard B. Buxton in understanding MR perfusion and lung water measurements are gratefully acknowledged.

GRANTS

This study was supported by American Heart Association Grant 0540002N, and National Institutes of Health Grants R01-HL081171–01A1, R01-HL-64741, R01-HL-077241–02, and P41-RR02305.

REFERENCES

1. **Abboud M, Sinatra A, Maître X, Tastevin G, Nacher PJ.** High nuclear polarization of ^{3}He at low and high pressure by metastability exchange optical pumping at 1.5 Tesla. *Europhys Lett* 68: 480–486, 2004.
2. **Albert MS, Cates GD, Driehuys B, Happer W, Saam B, Springer CS Jr, Wishnia A.** Biological magnetic resonance imaging using laser-polarized ^{129}Xe. *Nature* 370: 199–201, 1994.
3. **Altemeier WA, McKinney S, Glenny RW.** Fractal nature of regional ventilation distribution. *J Appl Physiol* 88: 1551–1557, 2000.
4. **Altes TA, Powers PL, Knight-Scott J, Rakes G, Platts-Mills TA, de Lange EE, Alford BA, Mugler JP 3rd, Brookeman JR.** Hyperpolarized

^{3}He MR lung ventilation imaging in asthmatics: preliminary findings. *J Magn Reson Imaging* 13: 378–384, 2001.

5. **Amis TC, Jones HA, Hughes JM.** Effect of posture on inter-regional distribution of pulmonary perfusion and $\dot{V}_A/\dot{Q}$ ratios in man. *Respir Physiol* 56: 169–182, 1984.
6. **Arnold JF, Fidler F, Wang T, Pracht ED, Schmidt M, Jakob PM.** Imaging lung function using rapid dynamic acquisition of T1-maps during oxygen enhancement. *MAGMA* 16: 246–253, 2004.
7. **Bayat S, Le Duc G, Porra L, Berruyer G, Nemoz C, Monfraix S, Fiedler S, Thomlinson W, Suortti P, Standertskjold-Nordenstam CG, Sovijarvi AR.** Quantitative functional lung imaging with synchrotron radiation using inhaled xenon as contrast agent. *Phys Med Biol* 46: 3287–3299, 2001.
8. **Berthezene Y, Vexler V, Clement O, Muhler A, Moseley ME, Brasch RC.** Contrast-enhanced MR imaging of the lung: assessments of ventilation and perfusion. *Radiology* 183: 667–672, 1992.
9. **Bolar DS, Levin DL, Hopkins SR, Frank LF, Liu TT, Wong EC, Buxton RB.** Quantification of regional pulmonary blood flow using ASL-FAIRER. *Magn Reson Med* 55: 1308–1317, 2006.
10. **Briguori C, Colombo A, Airoldi F, Melzi G, Michev I, Carlino M, Montorfano M, Chieffo A, Bellanca R, Ricciardelli B.** Gadolinium-based contrast agents and nephrotoxicity in patients undergoing coronary artery procedures. *Catheter Cardiovasc Interv* 67: 175–180, 2006.
11. **Brudin LH, Rhodes CG, Valind SO, Jones T, Hughes JM.** Interrelationships between regional blood flow, blood volume, and ventilation in supine humans. *J Appl Physiol* 76: 1205–1210, 1994.
12. **Brudin LH, Rhodes CG, Valind SO, Wollmer P, Hughes JM.** Regional lung density and blood volume in nonsmoking and smoking subjects measured by PET. *J Appl Physiol* 63: 1324–1334, 1987.
13. **Buxton R.** *Introduction to Functional Magnetic Resonance Imaging: Principals and Techniques*. Cambridge, UK: Cambridge University Press, 2002.
14. **Chen XJ, Moller HE, Chawla MS, Cofer GP, Driehuys B, Hedlund LW, Johnson GA.** Spatially resolved measurements of hyperpolarized gas properties in the lung in vivo. I. Diffusion coefficient. *Magn Reson Med* 42: 721–728, 1999.
15. **Colegrove F, Schearer L, Walters G.** Polarization of ^{3}He gas by optical pumping. *Physiol Rev* 132: 2561–2572, 1963.
16. **Cutillo AG, Morris AH, Blatter DD, Case TA, Ailion DC, Durney CH, Johnson SA.** Determination of lung water content and distribution by nuclear magnetic resonance. *J Appl Physiol* 57: 583–588, 1984.
17. **Deninger AJ, Eberle B, Bermuth J, Escat B, Markstaller K, Schmiedeskamp J, Schreiber WG, Surkau R, Otten E, Kauczor HU.** Assessment of a single-acquisition imaging sequence for oxygen-sensitive ^{3}He-MRI. *Magn Reson Med* 47: 105–114, 2002.
18. **Deninger AJ, Eberle B, Ebert M, Grossmann T, Heil W, Kauczor H, Lauer L, Markstaller K, Otten E, Schmiedeskamp J, Schreiber W, Surkau R, Thelen M, Weiler N.** Quantification of regional intrapulmonary oxygen partial pressure evolution during apnea by ^{3}He MRI. *J Magn Reson* 141: 207–216, 1999.
19. **Deninger AJ, Mansson S, Petersson JS, Pettersson G, Magnusson P, Svensson J, Fridlund B, Hansson G, Erjefeldt I, Wollmer P, Golman K.** Quantitative measurement of regional lung ventilation using ^{3}He MRI. *Magn Reson Med* 48: 223–232, 2002.
20. **Dietrich O, Losert C, Attenberger U, Fasol U, Peller M, Nikolaou K, Reiser MF, Schoenberg SO.** Fast oxygen-enhanced multislice imaging of the lung using parallel acquisition techniques. *Magn Reson Med* 53: 1317–1325, 2005.
21. **Eberle B, Markstaller K, Schreiber WG, Kauczor HU.** Hyperpolarised gases in magnetic resonance: a new tool for functional imaging of the lung. *Swiss Med Wkly* 131: 503–509, 2001.
22. **Eberle B, Weiler N, Markstaller K, Kauczor H, Deninger A, Ebert M, Grossmann T, Heil W, Lauer LO, Roberts TP, Schreiber WG, Surkau R, Dick WF, Otten EW, Thelen M.** Analysis of intrapulmonary O_2 concentration by MR imaging of inhaled hyperpolarized helium-3. *J Appl Physiol* 87: 2043–2052, 1999.
23. **Elmstahl B, Nyman U, Leander P, Chai CM, Golman K, Bjork J, Almen T.** Gadolinium contrast media are more nephrotoxic than iodine media. The importance of osmolality in direct renal artery injections. *Eur Radiol* 16: 2712–2720, 2006.
24. **Fain SB, Altes TA, Panth SR, Evans MD, Waters B, Mugler JP, 3rd Korosec FR, Grist TM, Silverman M, Salerno M, Owers-Bradley J.** Detection of age-dependent changes in healthy adult lungs with diffusion-weighted ^{3}He MRI. *Acad Radiol* 12: 1385–1393, 2005.
25. **Fain SB, Panth SR, Evans MD, Wentland AL, Holmes JH, Korosec FR, O'Brien MJ, Fountaine H, Grist TM.** Early emphysematous changes in asymptomatic smokers: detection with ^{3}He MR imaging. *Radiology* 239: 875–883, 2006.
26. **Fischer MC, Spector ZZ, Ishii M, Yu J, Emami K, Itkin M, Rizi R.** Single-acquisition sequence for the measurement of oxygen partial pressure by hyperpolarized gas MRI. *Magn Reson Med* 52: 766–773, 2004.
27. **Frank LR, Wong EC, Haseler LJ, Buxton RB.** Dynamic imaging of perfusion in human skeletal muscle during exercise with arterial spin labeling. *Magn Reson Med* 42: 258–267, 1999.
28. **Gentile T, Hayden M, Barlow M.** Comparison of metastability-exchange optical pumping sources. *J Opt Soc Am A* 20: 2068–2074, 2003.
29. **Glaister DH.** The effect of posture on the distribution of ventilation and blood flow in the normal lung. *Clin Sci* 33: 391–398, 1967.
30. **Glenny RW.** Heterogeneity in the lung: concepts and measures. In: *Complexity in Structure and Function in the Lung*, edited by Hlastala MP and Robertson HT. New York: Dekker, 1998, p. 571–609.
31. **Glenny RW, Bernard S, Robertson HT, Hlastala MP.** Gravity is an important but secondary determinant of regional pulmonary blood flow in upright primates. *J Appl Physiol* 86: 623–632, 1999.
32. **Glenny RW, Lamm WJ, Albert RK, Robertson HT.** Gravity is a minor determinant of pulmonary blood flow distribution. *J Appl Physiol* 71: 620–629, 1991.
33. **Haage P, Karaagac S, Spuntrup E, Truong HT, Schmidt T, Gunther RW.** Feasibility of pulmonary ventilation visualization with aerosolized magnetic resonance contrast media. *Invest Radiol* 40: 85–88, 2005.
34. **Haczku A, Emami K, Fischer MC, Kadlecek S, Ishii M, Panettieri RA, Rizi RR.** Hyperpolarized ^{3}He MRI in asthma measurements of regional ventilation following allergic sensitization and challenge in mice–preliminary results. *Acad Radiol* 12: 1362–1370, 2005.
35. **Happer W.** Optical pumping. *Rev Mod Phys* 44: 169–249, 1972.
36. **Happer W, Miron E, Schaefer S, Schreiber D, Wijngaarden W, Zeng X.** Polarization of the nuclear spins of noble-gas atoms by spin-exchange with optically pumped alkali-metal atoms. *Phys Rev A* 29: 3092–3110, 1984.
37. **Hatabu H, Tadamura E, Levin DL, Chen Q, Li W, Kim D, Prasad PV, Edelman RR.** Quantitative assessment of pulmonary perfusion with dynamic contrast-enhanced MRI. *Magn Reson Med* 42: 1033–1038, 1999.
38. **Hayes CE, Case TA, Ailion DC, Morris AH, Cutillo A, Blackburn CW, Durney CH, Johnson SA.** Lung water quantitation by nuclear magnetic resonance imaging. *Science* 216: 1313–1315, 1982.
39. **Henderson AC, Levin DL, Hopkins SR, Olfert IM, Buxton RB, Prisk GK.** Steep head-down tilt has persisting effects on the distribution of pulmonary blood flow. *J Appl Physiol* 101: 583–589, 2006.
40. **Hlastala MP, Lamm WJ, Karp A, Polissar NL, Starr IR, Glenny RW.** Spatial distribution of hypoxic pulmonary vasoconstriction in the supine pig. *J Appl Physiol* 96: 1589–1599, 2004.
41. **Hopkins SR, Garg J, Bolar DS, Balouch J, Levin DL.** Pulmonary blood flow heterogeneity during hypoxia and high-altitude pulmonary edema. *Am J Respir Crit Care Med* 171: 83–87, 2005.
42. **Hopkins SR, Gavin TP, Siafakas NM, Haseler LJ, Olfert IM, Wagner H, Wagner PD.** Effect of prolonged, heavy exercise on pulmonary gas exchange in athletes. *J Appl Physiol* 85: 1523–1532, 1998.
43. **Hughes JM, Glazier JB, Maloney JE, West JB.** Effect of lung volume on the distribution of pulmonary blood flow in man. *Respir Physiol* 4: 58–72, 1968.
44. **Jakob PM, Wang T, Schultz G, Hebestreit H, Hebestreit A, Hahn D.** Assessment of human pulmonary function using oxygen-enhanced T(1) imaging in patients with cystic fibrosis. *Magn Reson Med* 51: 1009–1016, 2004.
45. **Johnson RLJ, Spicer WS, Bishop JM, Forster RE.** Pulmonary capillary blood volume, flow and diffusing capacity during exercise. *J Appl Physiol* 15: 893–902, 1960.
46. **Kastler A.** Quelques suggestions concernant la production optique et la détection optique d'une inégalité de population des niveaux de quantification spatiale des atomes. Application a l'éxperience de Stern et Gerlach et a la résonance magnétique. *J Physique Rad* 11: 255–265, 1950.
47. **Kauczor HU, Chen XJ, van Beek EJ, Schreiber WG.** Pulmonary ventilation imaged by magnetic resonance: at the doorstep of clinical application. *Eur Respir J* 17: 1008–1023, 2001.
48. **Kauczor HU, Hofmann D, Kreitner KF, Nilgens H, Surkau R, Heil W, Potthast A, Knopp MV, Otten EW, Thelen M.** Normal and abnormal pulmonary ventilation: visualization at hyperpolarized He-3 MR imaging. *Radiology* 201: 564–568, 1996.

49. **Kauczor HU, Kreitner KF.** MRI of the pulmonary parenchyma. *Eur Radiol* 9: 1755–1764, 1999.
50. **Kilian W, Seifert F, Rinneberg H.** Dynamic NMR spectroscopy of hyperpolarized ^{129}Xe in human brain analyzed by an uptake model. *Magn Reson Med* 51: 843–847, 2004.
51. **Kosuda S, Kobayashi H, Kusano S.** Change in regional pulmonary perfusion as a result of posture and lung volume assessed using technetium-99m macroaggregated albumin SPET. *Eur J Nucl Med* 27: 529–535, 2000.
52. **Lauterbur P.** Image formation by induced local interactions: examples of employing nuclear magnetic resonance. *Nature* 242: 190–191, 1973.
53. **Leawoods J, Yablonskiy D, Saam B, Gierada D, Conradi MS.** Hyperpolarized ^{3}He gas production and MR imaging of the lung. *Concept Magn Reson* 13: 277–293, 2001.
54. **Levin DL, Chen Q, Zhang M, Edelman RR, Hatabu H.** Evaluation of regional pulmonary perfusion using ultrafast magnetic resonance imaging. *Magn Reson Med* 46: 166–171, 2001.
55. **Levin DL, Hatabu H.** MR evaluation of pulmonary blood flow. *J Thorac Imaging* 19: 241–249, 2004.
56. **MacFall JR, Charles HC, Black RD, Middleton H, Swartz JC, Saam B, Driehuys B, Erickson C, Happer W, Cates GD, Johnson GA, Ravin CE.** Human lung air spaces: potential for MR imaging with hyperpolarized He-3. *Radiology* 200: 553–558, 1996.
57. **Mai VM.** Hyperpolarized gas and oxygen-enhanced magnetic resonance imaging. *Methods Mol Med* 124: 325–345, 2006.
58. **Mai VM, Berr SS.** MR perfusion imaging of pulmonary parenchyma using pulsed arterial spin labeling techniques: FAIRER and FAIR. *J Magn Reson Imaging* 9: 483–487, 1999.
59. **Månsson S.** *Hyperpolarized Nuclei for NMR Imaging and Spectroscopy.* Malmo, Sweden: Malmö University Hospital & Lund Institute of Technology, 2002.
60. **Mansson S, Deninger AJ, Magnusson P, Pettersson G, Olsson LE, Hansson G, Wollmer P, Golman K.** ^{3}He MRI-based assessment of posture-dependent regional ventilation gradients in rats. *J Appl Physiol* 98: 2259–2267, 2005.
61. **Mayo JR, MacKay AL, Whittall KP, Baile EM, Pare PD.** Measurement of lung water content and pleural pressure gradient with magnetic resonance imaging. *J Thorac Imaging* 10: 73–81, 1995.
62. **McKenzie DC, O'Hare TJ, Mayo J.** The effect of sustained heavy exercise on the development of pulmonary edema in trained male cyclists. *Respir Physiol Neurobiol* 145: 209–218, 2005.
63. **Mentore K, Froh DK, de Lange EE, Brookeman JR, Paget-Brown AO, Altes TA.** Hyperpolarized HHe 3 MRI of the lung in cystic fibrosis: assessment at baseline and after bronchodilator and airway clearance treatment. *Acad Radiol* 12: 1423–1429, 2005.
64. **Misselwitz B, Muhler A, Heinzelmann I, Bock JC, Weinmann HJ.** Magnetic resonance imaging of pulmonary ventilation. Initial experiences with a gadolinium-DTPA-based aerosol. *Invest Radiol* 32: 797–801, 1997.
65. **Moller HE, Chen XJ, Saam B, Hagspiel KD, Johnson GA, Altes TA, de Lange EE, Kauczor HU.** MRI of the lungs using hyperpolarized noble gases. *Magn Reson Med* 47: 1029–1051, 2002.
66. **Moller HE, Hedlund LW, Chen XJ, Carey MR, Chawla MS, Wheeler CT, Johnson GA.** Measurements of hyperpolarized gas properties in the lung. Part III: (3)He T(1). *Magn Reson Med* 45: 421–430, 2001.
67. **Morbach AE, Gast KK, Schmiedeskamp J, Dahmen A, Herweling A, Heussel CP, Kauczor HU, Schreiber WG.** Diffusion-weighted MRI of the lung with hyperpolarized helium-3: a study of reproducibility. *J Magn Reson Imaging* 21: 765–774, 2005.
68. **Mure M, Domino KB, Lindahl SG, Hlastala MP, Altemeier WA, Glenny RW.** Regional ventilation-perfusion distribution is more uniform in the prone position. *J Appl Physiol* 88: 1076–1083, 2000.
69. **Naish JH, Parker GJ, Beatty PC, Jackson A, Young SS, Waterton JC, Taylor CJ.** Improved quantitative dynamic regional oxygen-enhanced pulmonary imaging using image registration. *Magn Reson Med* 54: 464–469, 2005.
70. **Ohno Y, Hatabu H, Higashino T, Nogami M, Takenaka D, Watanabe H, Van Cauteren M, Yoshimura M, Satouchi M, Nishimura Y, Sugimura K.** Oxygen-enhanced MR imaging: correlation with postsurgical lung function in patients with lung cancer. *Radiology* 236: 704–711, 2005.
71. **Pracht ED, Arnold JF, Wang T, Jakob PM.** Oxygen-enhanced proton imaging of the human lung using T2. *Magn Reson Med* 53: 1193–1196, 2005.
72. **Rizi RR, Baumgardner JE, Ishii M, Spector ZZ, Edvinsson JM, Jalali A, Yu J, Itkin M, Lipson DA, Gefter W.** Determination of regional $\dot{V}_A/\dot{Q}$ by hyperpolarized ^{3}He MRI. *Magn Reson Med* 52: 65–72, 2004.
73. **Roberts DA, Detre JA, Bolinger L, Insko EK, Lenkinski RE, Pentecost MJ, Leigh JS Jr.** Renal perfusion in humans: MR imaging with spin tagging of arterial water. *Radiology* 196: 281–286, 1995.
74. **Ruppert K, Mata JF, Brookeman JR, Hagspiel KD, Mugler JP 3rd.** Exploring lung function with hyperpolarized ^{129}Xe nuclear magnetic resonance. *Magn Reson Med* 51: 676–687, 2004.
75. **Saam BT, Yablonskiy DA, Kodibagkar VD, Leawoods JC, Gierada DS, Cooper JD, Lefrak SS, Conradi MS.** MR imaging of diffusion of ^{3}He gas in healthy and diseased lungs. *Magn Reson Med* 44: 174–179, 2000.
76. **Salerno M, Altes TA, Brookeman JR, de Lange EE, Mugler JP 3rd.** Rapid hyperpolarized ^{3}He diffusion MRI of healthy and emphysematous human lungs using an optimized interleaved-spiral pulse sequence. *J Magn Reson Imaging* 17: 581–588, 2003.
77. **Samee S, Altes T, Powers P, de Lange EE, Knight-Scott J, Rakes G, Mugler JP 3rd, Ciambotti JM, Alford BA, Brookeman JR, Platts-Mills TA.** Imaging the lungs in asthmatic patients by using hyperpolarized helium-3 magnetic resonance: assessment of response to methacholine and exercise challenge. *J Allergy Clin Immunol* 111: 1205–1211, 2003.
78. **Sasse SA, Berry RB, Nguyen TK, Light RW, Mahutte CK.** Arterial blood gas changes during breath-holding from functional residual capacity. *Chest* 110: 958–964, 1996.
79. **Shellock FG, Kanal E.** Safety of magnetic resonance imaging contrast agents. *J Magn Reson Imaging* 10: 477–484, 1999.
80. **Stejskal E.** Use of spin echoes in a pulsed magnetic field gradient to study anisotrophic restricted diffusion and flow. *J Chem Phys* 43: 3597–3603, 1965.
81. **Suga K, Ogasawara N, Okada M, Matsunaga N, Arai M.** Regional lung functional impairment in acute airway obstruction and pulmonary embolic dog models assessed with gadolinium-based aerosol ventilation and perfusion magnetic resonance imaging. *Invest Radiol* 37: 281–291, 2002.
82. **Suga K, Ogasawara N, Tsukuda T, Matsunaga N.** Assessment of regional lung ventilation in dog lungs with Gd-DTPA aerosol ventilation MR imaging. *Acta Radiol* 43: 282–291, 2002.
83. **Swenson ER, Domino KB, Hlastala MP.** Physiological effects of oxygen and carbon dioxide on $\dot{V}_A/\dot{Q}$ heterogeneity. In: *Complexity in Structure and Function in the Lung*, edited by Hlastala MP and Robertson HT. New York: Dekker, 1998, p. 511–547.
84. **Thompson HK Jr, Starmer CF, Whalen RE, McIntosh HD.** Indicator transit time considered as a gamma variate. *Circ Res* 14: 502–515, 1964.
85. **Walker T, Happer W.** Spin-exchange optical pumping of noble-gas nuclei. *Rev Mod Phys* 69: 629–642, 1997.
86. **Weisskoff RM, Chesler D, Boxerman JL, Rosen BR.** Pitfalls in MR measurement of tissue blood flow with intravascular tracers: which mean transit time? *Magn Reson Med* 29: 553–558, 1993.
87. **West JB.** Gravity and pulmonary blood flow distribution. *J Appl Physiol* 73: 2201–2202, 1992.
88. **Whipp BJ.** Dynamics of pulmonary gas exchange. *Circulation* 76: VI18–VI28, 1987.
89. **Whitelaw WA, McBride B, Ford GT.** Effect of lung volume on breath holding. *J Appl Physiol* 62: 1962–1969, 1987.
90. **Wilke N, Jerosch-Herold M, Stillman AE, Kroll K, Tsekos N, Merkle H, Parrish T, Hu X, Wang Y, Bassingthwaighte J, et al.** Concepts of myocardial perfusion imaging in magnetic resonance imaging. *Magn Reson Q* 10: 249–286, 1994.
91. **Wong EC, Buxton RB, Frank LR.** Quantitative imaging of perfusion using a single subtraction (QUIPSS and QUIPSS II). *Magn Reson Med* 39: 702–708, 1998.
92. **Yablonskiy DA, Sukstanskii AL, Leawoods JC, Gierada DS, Bretthorst GL, Lefrak SS, Cooper JD, Conradi MS.** Quantitative in vivo assessment of lung microstructure at the alveolar level with hyperpolarized ^{3}He diffusion MRI. *Proc Natl Acad Sci USA* 99: 3111–3116, 2002.
93. **Yang J, Wan M, Guo Y.** Pulmonary functional MRI: an animal model study of oxygen-enhanced ventilation combined with Gd-DTPA-enhanced perfusion. *Chin Med J (Engl)* 117: 1489–1496, 2004.